Periodica Polytechnica
Civil Engineering

59(4), pp. 575–582, 2015
DOI: 10.3311/PPci.8173

RESEARCH ARTICLE

A Simulation Model for Determining the Mechanical Properties of Rapeseed using the Discrete Element Method

Kornél Tamás, *Bernát* Földesi, *János Péter* Rádics, *István J.* Jóri, *László* Fenyvesi

Received 22-04-2015, revised 22-06-2015, accepted 07-09-2105

Abstract

This paper describes the mechanical modeling of rapeseed using the 3D Discrete Element Method (DEM). We investigated rapeseeds as a set of granular material points using a linear elastic material model with Coulomb friction and cohesive bonds. The parameters of the model were determined through physical and mechanical investigations. The mechanical properties were validated against actual measurement results using a single-axis compression box and a direct shear box. The investigations yielded the following micro-mechanical parameters: normal particle stiffness (Kn): 437 kN/m; particle shear stiffness (Ks): 100 kN/m; particle-to-particle friction coefficient (μ) 0.5; particle-to-wall friction coefficient (μ) 0.2; wall normal stiffness (Kn): 1311 kN/m; wall shear stiffness (Ks): 300 kN/m; local damping coefficient (γ): 0.7. The results proved that the DEM method is suitable for simulating the macro-mechanical behavior of rapeseed for the pressing process.

Keywords

rapeseed · material model · discrete element method · DEM · compression · direct shear box test · calibration

Kornél Tamás

Department of Machine and Product Design, Faculty of Mechanical Engineering, Budapest University of Technology and Economics, H-1111 Budapest, Bertalan Lajos u. 1., Hungary
e-mail: tamas.kornel@gt3.bme.hu

Bernát Földesi
János Péter Rádics
István J. Jóri

Department of Machine and Product Design, Faculty of Mechanical Engineering, Budapest University of Technology and Economics, H-1111 Budapest, Bertalan Lajos u. 1., Hungary

László Fenyvesi

NARIC Institute of Agricultural Engineering, H-2100 Gödöllő, Tessedik Sámuel u. 4., Hungary

1 Introduction

Our planet's fossil energy resources are finite, so renewable energy resources, including biofuels like biodiesel, play an increasingly vital role. Biodiesel is made from vegetable oils, and one of its key base materials is rapeseed oil pressed from rapeseed (Brassica napus L.). Rapeseed oil is used both as a fuel and as a base material in the food and chemical industry. Efforts are made in the production process to improve the properties of the resulting oil. The properties of the oil can be improved by cross-breeding, genetic modifications, more efficient plant care, pretreatment of harvested seeds, improved oil extraction technologies and physical/chemical post-treatment of the extracted oil. During mechanical processing, the most important property is the material behavior of rapeseed under normal and shear stresses applied during processing.

From a mechanical engineering point of view, the focus is on the extraction process where different methods can be used to separate the oil from the solid parts [1]. The mechanical designs used rely on an empirical or experimental basis that, however, does not provide detailed insights into what exactly happens during the process [2]. In order to create more efficient designs, new procedures need to be developed. Owing to its granular material properties, rapeseed exhibits a characteristic mechanical behavior [3].

The particle geometry of granular agricultural materials greatly determines their technological processing [4]. A complete description of the generally irregular grain shape would require too many measurement data. However, practice teaches us that a good approximation of particle geometry can be achieved using well-selected orthogonal sizes for length, width, and thickness. An objective measure of grain shape is its sphericity, a measure that has various definitions. For smaller grain sizes, the simplest and most plausible method is to determine the largest inscribable and smallest circumscribable circle [5].

According to experience, certain properties of natural sets like granular agricultural materials show a Gaussian distribution, although log-normal distributions can also be found. The geometry is also characterized by the particle surface, which is important when studying the micro-mechanics of pressing, notably

surface adhesion. Granular materials can also be characterized by the volume, density, or unit weight of its particles. Materials with small grain sizes are usually characterized by their volume density (or unit weight) which, per definition, is mass per unit volume. Another property of granular materials is their porosity (void ratio), calculated as the ratio of voids (pore volume) to the total volume of the material [6].

The mechanical properties and behavior of biological materials are controlled by a host of factors [7]. Due to this complexity, theoretical approaches can only be used to approximate real-life behavior in special cases where certain conditions are met [8]. Therefore, empirical methods are mainly used, where the accurate recording of the factors determining material property and behavior is of key importance [9].

A number of researchers have investigated the parameters of material models using the Finite Element Method [10–12] and the Discrete Element Method [13, 14] for simulating agricultural soils [15–17]. Simulations using the Finite Element Method (FEM) to account for grain-to-grain phenomena in rapeseed do not provide sufficient accuracy.

In contrast, mechanical processes occurring during the processing of granular material can by analyzed with sufficient accuracy using a properly calibrated Discrete Element Method. DEM models used for this purpose were designed to fit the characteristics of the studied phenomenon and the properties of the materials to be simulated. The need to decrease resource requirements and simulation runtime justify the use of specialized models, but their usability for studying the various material phenomena is severely limited. While rapeseed material models designed in previous research were not validated with simulated multi-axis mechanical stresses, it is important to consider such stresses in order to account for the significant normal and shear stresses that occur during the extrusion pressing of rapeseed [18]. In order to investigate these more mechanically complex phenomena, more complex rapeseed models are needed that can be used to analyze multi-axis stresses within the grains. Earlier work in this field did not study complex multi-axis stress cases. During our research, we investigated the physical and mechanical properties of rapeseed, and used the results to design a mechanical model that reflects real material behavior.

2 Material and method

2.0.1 Measuring physical properties

The measurements were performed on cleaned rapeseed. Since the mechanical properties of biological materials are significantly influenced by their physical properties [19], we first determined the physical parameters of the sample under investigation [20]. Using a Dickey-john GAC 2100 Agri digital moisture tester, we measured the volume density of the sample as well as its moisture content and temperature. The size distribution of the seed sample was determined using a strainer measuring unit (MLW). Based on the geometry simplifications of the model, it was sufficient to only use loaders with 1.00, 1.25, 1.60, 2.00, 2.50, and 3.00 mm hole diameter for determining the size distribution required by the model. The masses of particles remaining on the strainers were measured using a Sartorius LA12005 digital weighing equipment. The fractions were determined in five measurements.

2.0.2 Single-axis compression tests

Mechanical behavior under single-axis load was investigated using a piston-operated compaction cylinder with an external/internal diameter of 100 / 80 mm [21]. The piston and its INSTRON 2525-802 load cell was mounted on the vertically moving slider of an INSTRON 5581 universal mechanical measurement instrument (UMM), with the compaction cylinder mounted on the mounting plate in accordance with the horizontal position of the piston (Fig. 1).

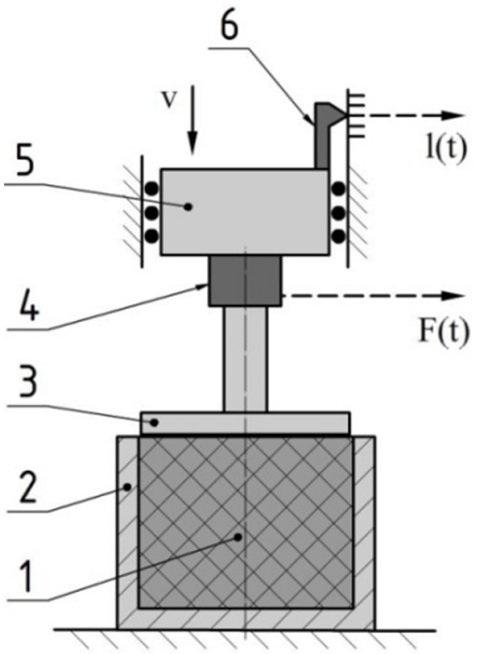

Fig. 1. Single-axis load test configuration (1. Sample tested; 2. Compaction cylinder; 3. Piston; 4. Load cell; 5. Slider; 6. Displacement sensor).

A desktop PC running the MERLIN software was used to log the data of the load cell. After loading the sample into the compaction cylinder, a constant piston feed rate was used to plot the compression curves. The measurement was performed there times, each time at a feed speed of 500 mm/minute. The compression curves so obtained were then averaged for compression force. Compression data were logged for a force range of 150 N - 30 kN (3.82 MPa).

2.0.3 Shear tests

The mechanical behavior of rapeseed under direct shear stress was investigated using a Balássy-type shear stress measuring unit [22] mounted on the UMM (Fig. 2). The first part, a baseplate with slots and rollers, was fixed to the mounting plate of the UMM. The movable lower half of the box with the load cell was placed on top of the baseplate. The top half of the shear box,

fixed to a pressure plate that could be moved vertically, was positioned above the lower half of the shear box. The internal dimensions of the shear box were $W = 200$ mm, $D = 200$ mm and $H = 80$ mm. A lever mechanism and applied weights ensured a constant pressure on the grain sample loaded into the shear box. The horizontally movable lower part was connected to the slider of the UMM by a wire reeved through a pulley.

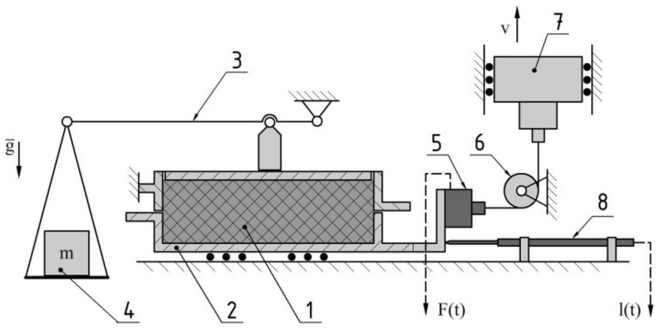

Fig. 2. Shear test configuration (1. Grain sample; 2. Shear box; 3. Load lever; 4. Load weight; 5. Load cell mounted on the shear box; 6. Pulley; 7. UMM slider ; 8. Displacement meter).

In order to minimize friction among the device's own components, a clearance of 1 mm was left between the fixed upper half and the movable lower half. A load cell type HBM U2A mounted on the lower part measured the traction force acting on the lower part, and the travel of the lower part was measured using a displacement meter. Signals from the measuring units were collected by an HBM Spider 8 data acquisition unit which forwarded them for storage to a portable computer running the Catman software. During the shear test measurements, a cross section of 200 mm x 200 mm of the seeds was investigated applying four different normal loads (25.75 kPa, 43.50 kPa, 61.00 kPa, 78.75 kPa) at a shear velocity of 3 mm/minute for each load. Based on the shear curves obtained for the different load values, we were able to determine the shear strengths, the macro-mechanical cohesions, and the internal friction angles [23]. In our evaluation, we also took into account the idle resistance of the shear box. Three measurements were performed for each measurement point. Seeds damaged by shearing were not reused in subsequent measurements.

2.1 Investigating the mechanical model of rapeseed using the DEM method

The rapeseed sample was modeled using the PFC^{3D} (Particle Flow Code in three dimensions) discrete element software [24]. The Discrete Element Method (DEM) is a numerical method for investigating the mechanical behavior of a large number of small particles. The method posits that the material consists of discrete particles that interact with each other though predefined connections and bonds among them. These bonds may break and new ones may be formed. Each of the finite number of particles has its own translational and rotational freedom, enabling it to perform translations and rotations by a finite amount [25]. The software is based on time steps and uses an explicit time integration algorithm. The model consists of infinitely rigid regular spherical particles, but allows particles pushed against each other to overlap.

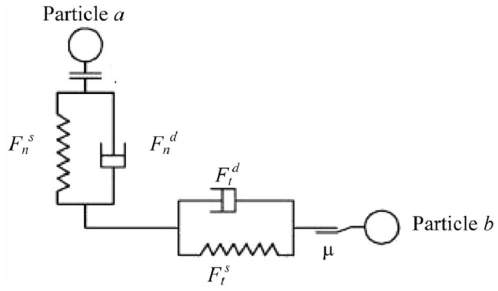

Fig. 3. Linear elastic contact model with Coulomb friction.

Connecting particle pairs are assumed to be in point contact. Contact faces important for studying the phenomenon can be modeled using planar elements of various types.

The material model for rapeseed was designed in multiple steps. In conjunction with DEM models, this process is called calibration [26]. The micromechanical model (the connections of particle pairs) provides a rough approximation for the behavior of the real material. The material model (particle set) was calibrated based on the results of the macro-mechanical tests (single-axis compression and shear tests). The immediate goal was to create a material model whose resistance values when subjected to macro-level compression and shear are close to those of the real material over the investigated interval [27]. This was achieved using a relatively simple linear elastic cohesive contact model with Coulomb friction (Fig. 3) and point-like contacts between pairs of spherical particles larger than the real seeds. The simplifications used when designing the model were necessary in order to reduce the runtime and computation intensity of the simulations and to fit the time and resources available for research.

When creating the model, first we specified the influence planes by their spatial orthogonal coordinates, then we generated the particle set consisting of spherical particles defined by their centers and their diameters. The generated particles and surface elements were assigned the initial parameters of the material model, and the gravitational acceleration vector was defined. The movements of the simulated particles were recalculated after each Δt time step, and its value was crucial to the usability of the simulation [28]. Depending on the material properties, the simulation model has a critical time step value, and choosing a value close to it or higher may cause simulation to work incorrectly. After each time step, the PFC^{3D} recalculated this critical time step value. A safety factor smaller than 1 was set to ensure that the value used during the simulation is a fraction of the critical time step value. With the time step value set correctly, the simulations yielded sufficiently accurate results.

2.2 Model for compression simulation

During calibration, a number of material parameters (cohesion, internal friction angle, friction) needed to be set correctly. Due to the complexity of the task, we ran the model separately for the different load cases. While all material properties affected the simulation results, their impact was different depending on the load case. When considering the effects of compression and shear, we assumed that the resistance shown by the particle set would primarily be governed by the rigidity of the particles during compression and by their friction and cohesivity during shear. The rolling resistance of regular spheres representing the seeds is significantly lower than that of real seeds this effect was compensated for by increasing the inter-particle friction coefficient and the particles' shear stiffness. Since compression load presses the particles together with a significant force, we could not entirely neglect the resistance caused by friction as particles slide on each other. We first used a linear elastic non-cohesive contact model with Coulomb friction to calibrate the normal stiffness and the internal friction coefficient. The initial parameters used are shown in Table 1. The particle–wall friction coefficient was set based on earlier rapeseed research.

Tab. 1. The model initial parameters.

Parameters	Values
Min. particle diameter (mm)	6
Max. particle diameter (mm)	7
Density of particles (kg m^{-3})	1250
Normal stiffness of the particle (kN m^{-1})	437
Shear stiffness of the particle (kN m^{-1})	100
Coefficient of friction (particle-particle) (-)	0.20
Coefficient of friction (particle-wall)	0.23
Normal stiffness of the wall (kN m^{-1})	4000
Shear stiffness of the wall (kN m^{-1})	1000
Coefficient of local damping (-)	0.7

The influence surfaces of the simulated compression cylinder are its internal envelope (Ø100 mm × 80 mm) and its bottom plate. The particle set, generated randomly into the cylindrical volume defined by the cylinder envelope (Ø100 mm × 200 mm), was settled using 9,81 m/s^2 gravitational acceleration to arrive at a steady state. Steady state was considered to have been reached once the unbalance force acting in the particle set reached 1 x 10^{-4} N. Particles located above the top rim of the envelope were discarded, then the surface representing the pressure plate of the piston was also defined. The model so obtained consisted of three surface elements and 2292 particles (Fig. 4). The number of discrete elements used was sufficient, as specifying the ratio between the largest and smallest particle was sufficient for describing the particle set. The material model using the chosen particle sizes (Table 1) was suitable for simulation purposes and also reduced the computational requirements.

During the simulations, the normal force acting on the piston face as a function of its displacement was determined at a constant piston feed rate of 500 mm/min. Data were logged for a load range of 150 N - 29.3 kN . We then reset the parameters of the material model and ran simulations to set the different calibration points defined by different combinations of normal stiffness [kN] and particle-particle friction coefficient [-] (300, 0.4; 400, 0.2; 400, 0.3; 400, 0.4; 400, 0.5; 500, 0.4; 600, 0.4). Using the particle set and its parameters, we determined the relationship between stiffness and friction, and calibrated the normal stiffness and the particle-particle friction coefficient.

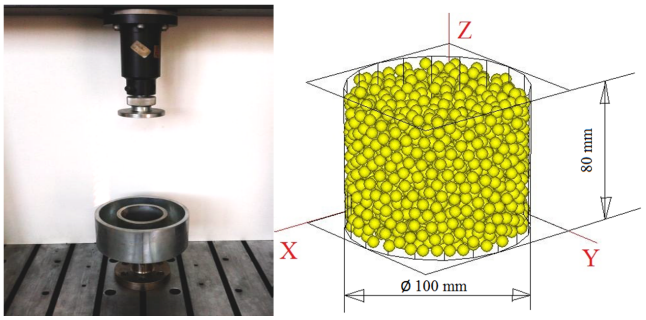

Fig. 4. The uniaxial compression test device, and the simulated oedometer test device in standby state (100 mm x 80 mm).

2.2.1 Model of the direct shear test

The shear resistance of the material model was mainly determined by the particle-particle friction coefficient and the normal (Cn) and shear (Cs) cohesional strength, with the latter two increasing the rolling resistance of the spherical particles. The friction coefficient was already set during the first stage, so the second stage was used to set the normal and shear parameters of the contact model positing point-like contacts. By increasing shear cohesion, we could increase the rolling resistance and also influence the internal friction angle of the material model. Setting the normal cohesion, we could define the proper macro-mechanical cohesion. The initial values of the material model used for the simulations are shown in Table 2.

Tab. 2. Parameters of shear simulation.

Parameters	Values
Min. particle diameter (mm)	6
Max. particle diameter (mm)	7
Density of particles (kg m^{-3})	1230
Normal stiffness of the particle (kN m^{-1})	384
Shear stiffness of the particle (kN m^{-1})	100
Normal strength of cohesion (N)	1.5
Shear strength of cohesion (N)	3.0
Coefficient of friction (particle-particle) (-)	0.34
Coefficient of friction (particle-wall)	0.23
Normal stiffness of the wall (kN m^{-1})	4000
Shear stiffness of the wall (kN m^{-1})	1000
Coefficient of local damping (-)	0.7

The influence surfaces of the shear box consisted of the internal surfaces of the two box halves (200 mm × 200 mm × 80 mm), their rims (200 mm × 40 mm), and the pressure plate. Once again, the particle set was randomly generated in the model space. Steady state was considered to have been reached once

the unbalance force acting in the settled particle set reached 1×10^{-3} N. The upper pressure plate was introduced into the model after settling, and discarding the surplus particles. The model so obtained consisted of 12 surface elements and 9805 particles (Fig. 5).

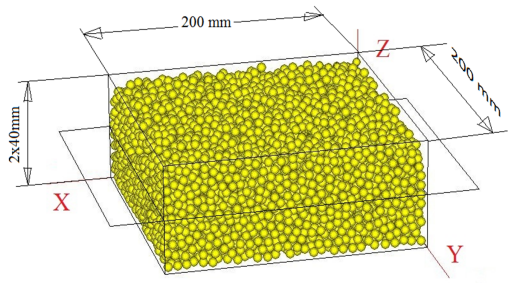

Fig. 5. The direct shear test equipment with the PC used for data acquisition, and the shear test model (200 mm × 200 mm × 80 mm).

In the first stage of the simulation, we applied a load equal to the real-life test through the upper compression plate. Once the upper compression plate reached its stationary state, we started pulling the bottom half of the box at a constant speed. Since the contact model did not include a viscosity component, we neglected the speed-dependence of the material's behavior. The runtime needed to simulate the relatively large number of particles could be decreased significantly by increasing the shear speed (300 mm/min), leaving the time step unchanged. Compared to the value used for shear tests (3 mm/min), the difference was relatively large, but the shear process was still too slow. The shear force was a signed sum of the normal and shear forces acting on the surfaces of the bottom half-box. Shear force values were recorded as a function of translation. The simulations lasted until a translation of 30 mm was reached. The points needed for calibration were defined by value pairs of normal (Cn) and shear (Cs) cohesional strength: 0.5, 3.0; 1.5, 2.0; 1.5, 3.0; 1.5, 4.0; 2.5, 3.0. For each of these combinations, simulations were run for the largest and smallest load (78.75 kPa and 25.75 kPa, respectively). The shear strength values were then determined based on the plotted shear curves and used to determine the macro-mechanical cohesion and the internal friction angle for each value combination. We then compared the results of the simulations with the actual measured results and calibrated the cohesion parameters of the model.

3 Results and discussion

3.1 Measurement results

The investigated rapeseed sample had a volume density (ρ) of 651 ± 3 kg/m^3, a temperature (t) of 24.3 ± 0.5 °C, and a moisture content (W%) of 5.5 ± 0.1 percent. Based on the results obtained using the strainer measuring unit, we determined the actual density function of the sample's particle sizes as well as the relative frequencies of particle sizes (Fig. 6). The results show that the majority of the particles fell into the size range of 1.7 - 2.0 mm. Considering the largest particle size of 7 mm used in the rapeseed material model, this corresponds to a 6 - 7 mm size range with linear distribution. The measured physical parameters agree with the results published in literature [2, 18].

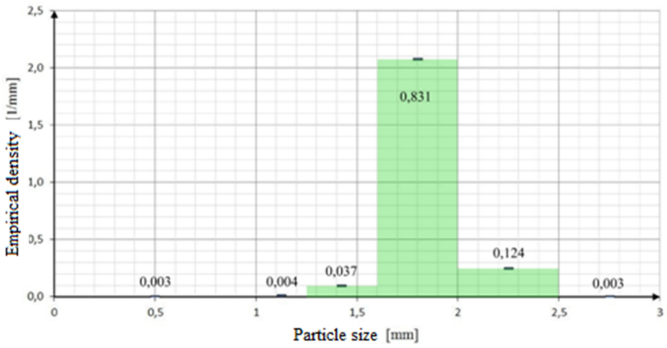

Fig. 6. Empirical rapeseed density function and fraction frequencies.

The compression curves obtained by applying a feed speed of 500 mm/min are shown in Fig. 7. While our study results obtained for single-axis compression could not be directly compared with results published in literature [21], because the measurement parameters used were different, the characteristic curves and the measured results were close to those obtained by other researchers, validating our tests. Since the curve points were plotted using the same x coordinates for all curves, averaging was performed based on the forces that caused the different deformation values. The curve obtained can be closely approximated using a second-order polynomial. In order to improve the approximation, the polynomial does not start from the origin. The resulting error caused in the origin was neglected. Because the polynomial is determined primarily by the linear and the quadratic coefficients, we used these two values during calibration for characterizing the curve.

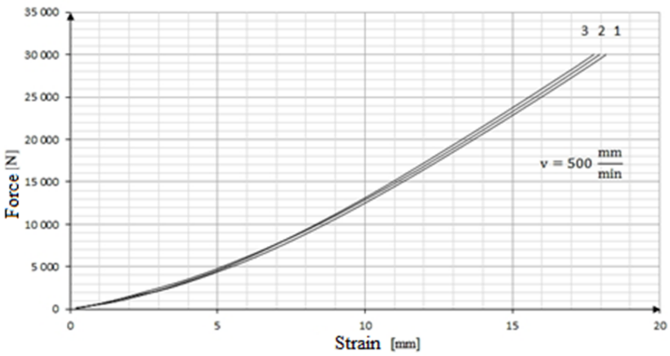

Fig. 7. Rapeseed compression curves ($v = 500$ mm/min).

The shear strength values were determined based on the stationary segments of the curves obtained from shear tests performed using different normal loads and a feed speed of 3 mm/min. The shear strength plotted as a function of normal stress defined the failure curve of the rapeseed (Fig. 8). Based on the line obtained, we could determine the macro-mechanical cohesion ($C = 11.41$ kPa) and the internal friction angle ($\Phi = 28.10°$). Cohesion among the initially dry seeds was caused by oil seeping to the seed surface as the sample was compressed. Using the material parameters determined by shear

tests yielded realistic results.

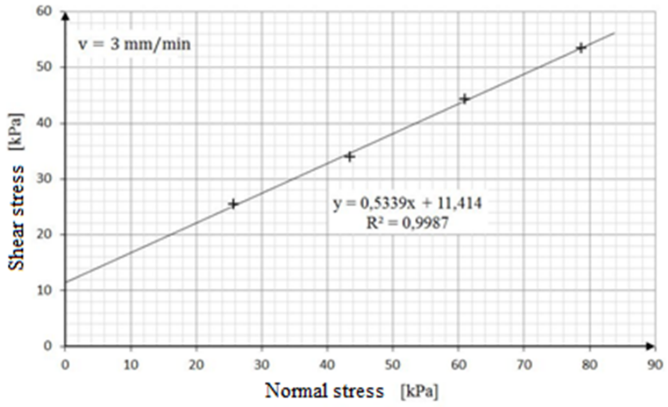

Fig. 8. The resulting σ - τ line of the direct shear test ($v = 3$ mm/min).

3.2 Calibration results of the rapeseed material model

The first calibration step was to set the volume density. In the compression model, the volume density of the settled and stationary sample was 661 kg/m^3, obtained using the initial parameters. In order to arrive at the desired value of 651 kg/m^3, we increased the particle density to 1230 kg/m^3.

The progressive characteristics of the curves obtained from compression simulation matched the measured values, but the deformation values of the simulated curves for a load of 150 N were larger than the measured ones. This difference was mainly caused by the simplicity of the model; the initial discarding of particles reaching above the cylinder rim resulted in a significant gap between the compression plate and the uppermost layer of the remaining particles. While this shifted the curves of compression simulation, the overall difference was less than 5% relative to the height of the simulated particle set. During analysis, the deformation values of the curves at a load of 150 N were assumed to be zero. Similarly to the measured compression curves, the simulated compression curves can be closely approximated using second-order polynomials ($R2 > 0.95$).

The curves were characterized using the linear and quadratic curve coefficients (Fig. 9). At the calibration points defined by value pairs of normal strength (Fig. 9a) and internal friction coefficient (Fig. 9b), the dependencies of the linear and quadratic curve coefficients were examined separately.

A planar regression surface could be fitted on each set of plotted points. The quadratic equations describing the surfaces can be assigned the corresponding coefficients of the measured curve. Equating the equations and the coefficients, we obtained an equation system with two unknown quantities. Solving these equations yielded a normal strength (Kn) of 384 kN/m and an internal friction coefficient (Φ) of 0.34. This concluded the compression calibration of the linear elastic cohesive contact model with Coulomb friction (Fig. 10).

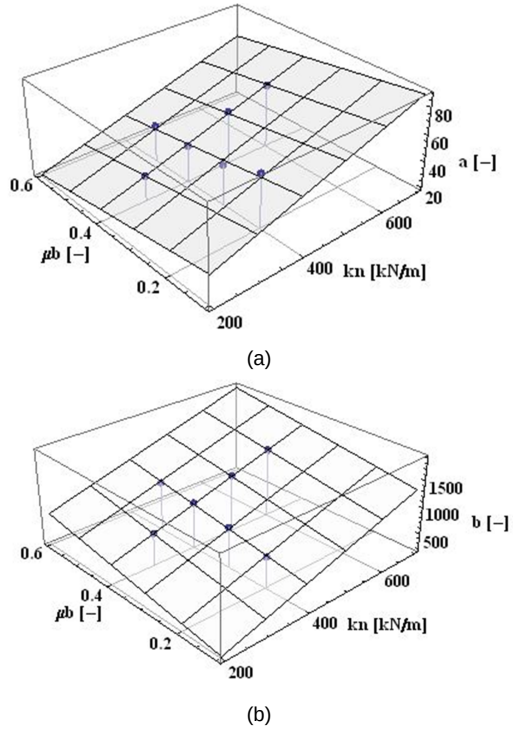

Fig. 9. Linear and quadratic curve coefficients of the second-order polynomials used to approximate the curves obtained from compression simulations, shown as a function of a, normal strength and b, internal friction coefficient.

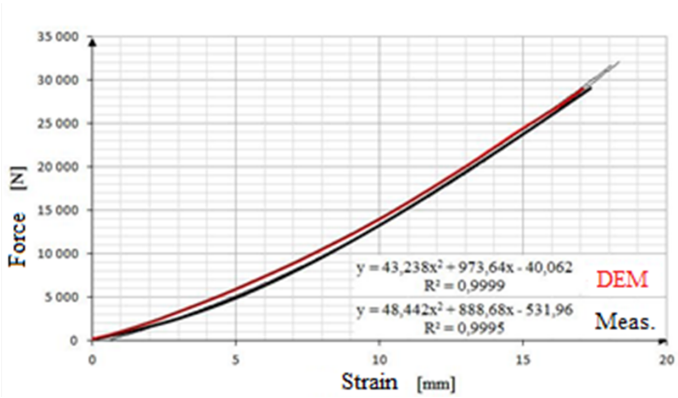

Fig. 10. The curve obtained after calibration based on measured and simulated compression tests.

3.3 The calibration of shear simulations

The shear simulations yielded degressive shear curves that matched the measured curves. The shear curves were evaluated using the method described for the measured curves. We determined the shear strengths for the different curves and plotted the values as a function of normal stress, enabling us to determine the macro-mechanical cohesion (C) (Fig. 11a) and the internal friction angle (Φ) (Fig. 11b).

At the calibration points defined by value pairs of normal strength and internal friction coefficient, we separately investigated the macro-mechanical cohesion and the tangent of the internal friction angle (Fig. 11).

Linear regression planes were fitted on the calibration points for both sets. The equations describing the surfaces can be assigned the macro-mechanical cohesion and the tangent of the

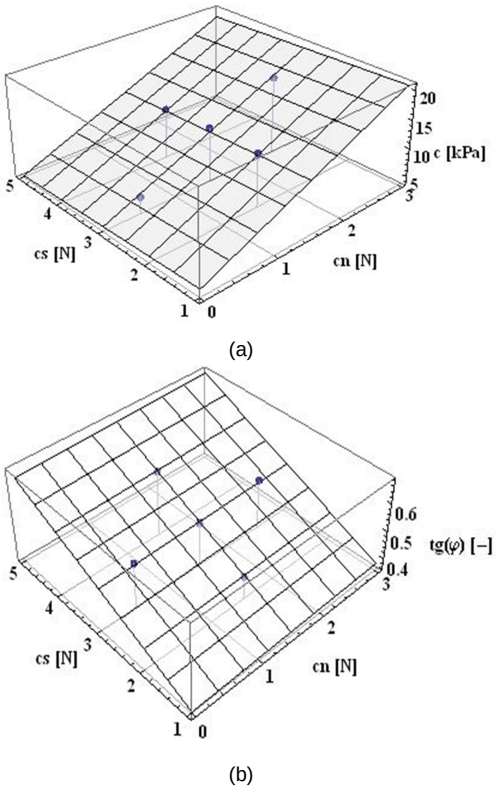

Fig. 11. The macro-mechanical parameters characteristic for the failure curves (a, cohesion; b, internal friction angle) obtained from shear simulations, shown as a function of the normal (Cn) and shear (Cs) cohesion components.

internal friction angle determined from the measurements. Solving the equation system with containing unknown quantities yielded 1.32 N for the normal component and 3.17 N for the shear component. The simulations run using these parameters approximated the measured failure curve, but the results were not satisfactory, so we fine-tuned the normal component of the model using linear interpolation between the calculated value pair and the 0.5, 3.0 calibration point. We finally obtained a rounded value of 1.1 N for the normal component and 3.2 N for the shear component. The results of the validate run are shown in Fig. 12 Shear simulations validated that the cohesive bond model can be used effectively for increasing the rolling resistance of spherical particles.

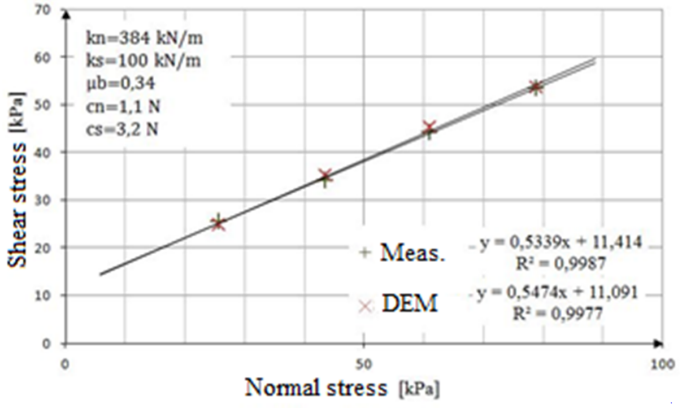

Fig. 12. Failure curves obtained using the model calibrated based on the results of measured and simulated shear tests.

As a last phase of calibration, the model was re-checked by running a compression simulation. The results show that the cohesive material model closely approximates the calibrated non-cohesive model (Fig. 13). The most noticeable difference between the curves is seen at a load value of 150 N. Due to the cohesion keeping the simulated particles together, the model begins to deform at a smaller load, but the curves still touch because the cohesion parameters can not be determined for single-axis load.

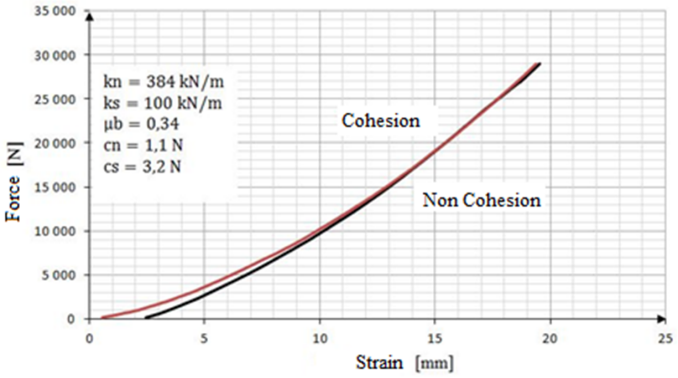

Fig. 13. Compression simulation results obtained for cohesive and non-cohesive material models.

4 Conclusions

Our research proved that the linear elastic cohesive contact model with Coulomb friction and point-like contacts can be used to create a material model that gives a good approximation of the macro-mechanical behavior of rapeseed. The physical and mechanical tests enabled us to calibrate the model for both compression and shear loads such that it exhibited a sufficiently good approximation of real-life behavior.

We also succeeded in determining the parameters based on the relationships among the calibration points. The DEM-based material model designed for rapeseed (studied at a temperature of $T = 24.5°C$ and a moisture content of $w = 5.5\%$) was validated for a maximum combined compression/shear load of 80 MPa, and for a maximum compression stress of 3.8 MPa. Since the contact model did not include a viscosity component, its mechanical behavior was not speed-dependent.

Using the micro-parameters obtained during calibration, a particle diameter of 7 mm, and a particle density of 1250 kg/m^3, we performed the oedometer test and validated a particle normal stiffness (Kn) of 437 kN/m, a particle shear stiffness (Ks) of 100 kN/m, a particle-particle friction coefficient (μ) of 0.5, and a particle-wall friction coefficient (μ) of 0.2. The validated results, i.e. the already mentioned micro-parameters of the direct shear box test were as follows: particle-particle cohesion strength in normal direction (Cn): 1.5 N; particle-particle shear strength (Cs): 3.1 N; wall stiffness in normal direction (Kn): 1311 kN/m; and wall shear stiffness (Ks): 300 kN/m, using a damping coefficient $\gamma = 0.7$.

The DEM modeling system is able to simulate many mechan-

ical principles of materials consisting of particles, making it possible to accurately analyze real-life phenomena. The 3D DEM method is suitable for the highly accurate simulation of a rapeseed set, as borne out by laboratory investigations.

We conclude that the DEM method is useful for modeling rapeseed as a set of particles in a linear elastic material model with Coulomb friction and point-like cohesive bonds. The results prove the accuracy and reliability of the DEM method, and the model we designed helps reduce the number of expensive measurements.

Acknowledgement

The authors gratefully acknowledge the assistance of the staff of the Hungarian Institute of Agricultural Engineering of Gödöllő for allowing the use of the soil bin testing facilities and provide the practical support during measurement. These researches were partially supported by the Hungarian Research Fund, under grant no. OTKA 48906.

References

1 **Raji AO, Favier JF**, *Model for the deformation in agricultural and food particulate materials under bulk compressive loading using discrete element method. I: Theory, model development and validation*, Journal of Food Engineering, **64**(3), (2004a), 359–371, DOI 10.1016/j.jfoodeng.2003.11.004.

2 **Tańska M, Rotkiewicz D, Kozirok W, Konopka I**, *Measurement of the geometrical features and surface colour of rapeseeds using digital image analysis*, Food Research International, **38**(7), (2005), 741–750, DOI 10.1016/j.foodres.2005.01.008.

3 **Raji AO, Favier JF**, *Model for the deformation in agricultural and food particulate materials under bulk compressive loading using discrete element method. II: Compression of oilseeds*, Journal of Food Engineering, **64**(3), (2004b), 373–380, DOI 10.1016/j.jfoodeng.2003.11.005.

4 **Bagi K**, *Geometrical modelling of granular assemblies*, Acta Technica Academiae Scientiarum Hungaricae, **107**(1-2), (1995), 1–16.

5 **Wiącek J, Molenda M, Horabik J, Ooi JY**, *Influence of grain shape and intergranular friction on material behavior in uniaxial compression: Experimental and DEM modelling*, Powder Technology, **217**, (2012), 435–442, DOI 10.1016/j.powtec.2011.10.060.

6 **Keppler I, Kocsis L, Oldal I, Farkas I, Csatar A**, *Grain velocity distribution in a mixed flow drye*, Advanced Powder Technology, **23**(6), (2012), 824–832, DOI 10.1016/j.apt.2011.11.003.

7 **Cundall PA, Strack ODL**, *A discrete numerical model for granular assemblies*, Geotechnique, **29**, (1979).

8 **Serrano AA, Rodriguez-Ortiz JM**, *A contribution to the mechanics of heterogeneous granular media*, Plasticity and Soil Mechanics 1973, Proc. Symp, 1973, pp. 215–227.

9 **Izli N, Unal H, Sincik M**, *Physical and mechanical properties of rapeseed at different moisture content*, International Agrophysics, **23**(2), (2009), 137–145.

10 **Fielke JM**, *Finite element modelling of the interaction of the cutting edge of tillage implements with soil*, Journal of Agricultural Engineering Research, **74**(1), (1999), 91–101, DOI 10.1006/jaer.1999.0440.

11 **Mouazen AM, Nemenyi M**, *Finite element analysis of subsoiler cutting in nonhomogeneous sandy loam soil*, Soil and Tillage Research, **51**, (1999), 1–15, DOI 10.1016/S0167-1987(99)00015-X.

12 **Kerényi G**, *A talaj vágásának modellezése végeselem módszerrel (Modelling of Soil Cutting with the Finite Element Method)*, PhD thesis, Polytechnic University of Budapest, Budapest; Budapest, HUNGARY, 1996. (in Hungarian).

13 **Sadek MA, Chen Y, Liu J**, *Simulating shear behavior of a sandy soil under different soil conditions*, Journal of Terramechanics, **48**(6), (2011), 451–458, DOI 10.1016/j.jterra.2011.09.006.

14 **Asaf Z, Rubinstein D, Shmulevich I**, *Determination of discrete element model parameters required for soil tillage*, Soil and Tillage Research, **92**(1-2), (2007), 227–242, DOI 10.1016/j.still.2006.03.006.

15 **Mustafa U, John MF, Chris S**, *Three-dimensional discrete element modelling of tillage: Determination of a suitable contact model and parameters for a cohesionless soil*, Biosystems Engineering, **121**(5), (2014), 105–117.

16 **Tamás K, Jóri JI**, *A talaj- kultivátorszerszám kapcsolat diszkrét elemes modellje. (The model of the soil- sweep interaction.)*, Mezőgazdasági technika, **55**(4), (2015), 4–5. (in Hungarian).

17 **Tamás K, Mouazen AM, Jóri JI**, *Investigation of the soil-tool interaction by DEM*, Soil and Tillage Research, **134**, (2013), 223–231, DOI 10.1016/j.still.2013.09.001.

18 **Çalışır S, Marakoğlu T, Öğüt H, Öztürk Ö**, *Physical properties of rapeseed (Brassica napus oleifera L.)*, Journal of Food Engineering, **61**(1), (2005), 61–66, DOI 10.1016/j.jfoodeng.2004.07.010.

19 **Sitkei G**, *Mechanics of agricultural materials*, Elsevier; Amsterdam, 1986.

20 **Wojtkowski M, Pecen J, Horabik J, Molenda M**, *Rapeseed impact against a flat surface: Physical testing and DEM simulation with two contact models*, Powder Technology, **198**(1), (2010), 61–68, DOI 10.1016/j.powtec.2009.10.015.

21 **Herak D, Kabutey A, Divisova M, Svatonova T**, *Comparison of the mechanical behavior of selected oilseeds under compression loading*, Notulae Botanicae Horti Agrobotanici Cluj-Napoca, **40**(2), (2012), 227–232.

22 **Balássy Z**, *Correction of data measured in a shear box*, Soil and Tillage Research, **19**(2-3), (1991), 165–173, DOI 10.1016/0167-1987(91)90084-B.

23 **Molenda M, Horabik J, Łukaszuk J, Wiącek J**, *Variability of intergranular friction and its role in DEM simulation of direct shear of an assembly of rapeseeds*, International Agrophysics, **25**(4), (2011), 361–368.

24 *Itasca, PFC3D Particle Flow Code in 3 Dimensions*, Itasca Consulting Group Inc; Minneapolis, MN, USA, 2008.

25 **Bagi K**, *An algorithm to generate random dense arrangements for discrete element simulations of granular assemblies*, Granular Matter, **7**(1), (2005), 31–43, DOI 10.1007/s10035-004-0187-5.

26 **Lawton PJ, Marchant JA**, *Direct shear testing of seeds in bulk*, Journal of Agricultural Engineering Research, **25**(2), (1980), 189–201, DOI 10.1016/0021-8634(80)90059-1.

27 **Wulfsohn D, Adams BA, Fredlund DG**, *Triaxial testing of unsaturated agricultural soils*, In: ASAE Paper No 94-1036. St. Joseph, 1994.

28 **Kruggel-Emden H, Sturm M, Wirtz S, Scherer V**, *Selection of an appropriate time integration scheme for the discrete element method (DEM)*, Computers & Chemical Engineering, **32**(10), (2008), 2263–2279, DOI 10.1016/j.compchemeng.2007.11.002.

29 **Wiącek J, Molenda M**, *Moisture-dependent physical properties of rapeseed – experimental and DEM modelling*, International Agrophysics, **25**(1), (2011), 59–65.